REVIEW ARTICLE

Neoplasia • Vol. 1, No. 3, August 1999, pp. 197–207 197

Available On-line at http://www.neoplasia.org

Causes and Effects of Heterogeneous Perfusion in Tumors[1]

Robert J. Gillies, Paul A. Schornack*, Timothy W. Secomb† and Natarajan Raghunand**

*Arizona Cancer Center; †Department of Physiology, University of Arizona, Tucson, AZ

Abstract

A characteristic of solid tumors is their heterogeneous distribution of blood flow, with significant hypoxia and acidity in low-flow regions. We review effects of heterogeneous tumor perfusion are reviewed and propose a conceptual model for its cause. Hypoxic-acidic regions are resistant to chemo- and radiotherapy and may stimulate progression to a more metastatic phenotype. In normal tissues, hypoxia and acidity induce angiogenesis, which is expected to improve perfusion. However, aggressive tumors can have high local microvessel density simultaneously with significant regions of hypoxia and acidosis. A possible explanation for this apparent contradiction is that the mechanisms regulating growth and adaptation of vascular networks are impaired. According to a recent theory for structural adaptation of vascular networks, four interrelated adaptive responses can work as a self-regulating system to produce a mature and efficient blood distribution system in normal tissues. It is proposed that heterogeneous perfusion in tumors may result from perturbation of this system. Angiogenesis may increase perfusion heterogeneity in tumors by increasing the disparity between parallel low- and high-resistance flow pathways. This conceptual model provides a basis for future rational therapies. For example, it indicates that selective destruction of tumor vasculature may increase perfusion efficiency and improve therapeutic efficacy.

Keywords: angiogenesis, perfusion, acid-base balance, hypoxia, VEEF, HIF-1.

Tumor Perfusion Is Heterogeneous

Tumor perfusion has long been recognized to be an important problem in clinical and experimental cancers (1–3). A hallmark of both clinical and experimental tumors is that they are heterogeneously perfused. This is illustrated in Figure 1, a magnetic resonance image (MRI) of an MCF-7 breast cancer xenograft growing in the mammary fat pad of a SCID mouse injected with a paramagnetic contrast agent, gadolinium-pentetic acid (Gd-DTPA) (Magnevist) (Berlex Lab, Wayne, NJ). This agent reduces the relaxation time of water protons, leading to higher signal intensity. Thus, at late time points after injection, brightness corresponds to regions with high vascular volume, high capillary permeability, and high extracellular space. As shown in this figure, the distribution of contrast agent is highly heterogeneous. Such heterogeneous patterns of enhancement are observable in both clinical (4) and experimental (5) tumors. A number of consequences follow from these observations. First, the pattern of enhancement visible by MRI likely predicts the pharmacokinetic distribution of chemotherapeutic drugs because it illustrates the portions of tumors that are accessible via blood perfusion (6–9). Second, the poorly perfused tumor regions are likely to be acidic and hypoxic, which can have important consequences for therapy and carcinogenesis (discussed later).

The time course of signal intensity enhancement with Gd-DTPA can be analyzed quantitatively by using dynamic enhanced magnetic resonance imaging (DEMRI), reviewed in Ref. (10). In this technique, signal intensity is monitored in time after a bolus injection of contrast agent. A time series of images is analyzed to generate enhancement curves for each of the 64,000 or so pixels in the image ("raw data" in Figure 2). Superficially, each enhancement curve contains two components, one corresponding to the arterial input function ("AIF," Figure 2) and the other corresponding to the net transfer of contrast agent from the vasculature to the interstitial space ("leak," Figure 2). Physiologically important values can be extracted from these curves that are related to the vascular volume, the cell volume, and the unidirectional exchange rate constant, k_{21} (11). The theory behind using these model-dependent analyses has been extensively discussed and will not be treated here (5,6,12–14). Alternatively, the data can be analyzed purely heuristically, generating values for lag time, time to maximally enhance, area under the curve, and so on. (15). Significant findings have been generated regardless of analytical method, indicating that DEMRI provides data that are robust and pathophysiologically important (10). For example, Knopp and colleagues (16) analyzed the same DEMRI data sets using both heuristic and model-dependent methods and concluded that the methods were equivalent in predicting response of cervical carcinoma to therapy. Importantly, DEMRI is increasingly being used to predict therapeutic response before there are frank changes in tumor morphology and, in some cases, before therapy has begun (16–23).

Tumor perfusion heterogeneity can also be demonstrated by more conventional methods, such as Doppler ultrasound (US) (24). With this technique, perfusion rates in a large

Address correspondence to: R.J. Gillies, Arizona Cancer Center, University of Arizona, Tucson, AZ 85724-5024. E-mail: gillies@u.arizona.edu

[1]Supported by NIH grants R01 CA77575-01 and T32 HL07249.

Received 11 May 1999; Accepted 27 May 1999.

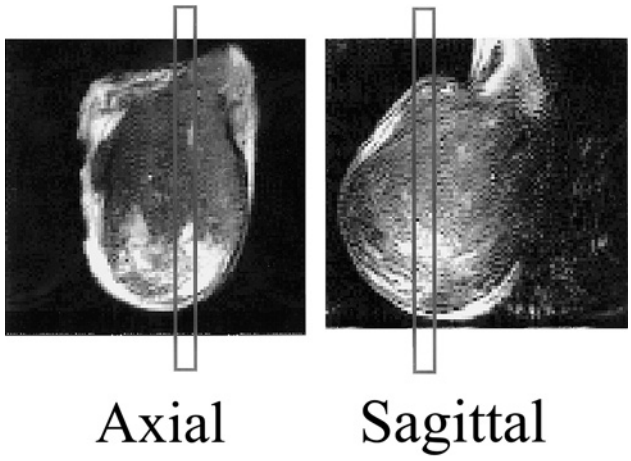

Figure 1. *Axial and sagittal sections through magnetic resonance image of MCF-7 human breast cancer xenograft growing in mammary fat pad of SCID mouse. Two minutes before acquisition of these T1-weighted images, the animal was injected with 27 μL Magnevist (Gd DTPA), which enhances thermal relaxation of spins, yielding higher signal intensities. The signal intensity is roughly proportional to the gadolinium concentration in each voxel.*

number of tumors and normal tissues have been determined (25). These studies have shown that blood perfusion in normal tissues is between 8 to 100 mL 100 g^{-1} min^{-1}. In contrast, perfusion in tumors can range from a high of 100 mL 100 g^{-1} min^{-1} to complete stasis. This low-end excursion of tumor perfusion indicates that regions exist that are very poorly perfused.

An additional method to measure tumor perfusion heterogeneity is the use of tumors grown in windowed chambers, either on the dorsal skin flap or in the ears of experimental animals (26–28). With this method, blood flow is monitored microscopically, often with fluorescently tagged erythrocytes, and blood velocity (in millimeters per minute) can be analyzed on a per-capillary basis. With such time-resolved imaging, the behavior of blood flow in tumors has been characterized as primarily being unstable, involving about 85% of all capillaries (29). Unstable blood flow indicates that blood flow in an individual capillary varies widely between very low and very high values (30,31). The remaining tumor capillaries are either totally static (about 1%), intermittently static (about 5%), or carry only plasma (i.e., no red blood cells, about 8%).

These studies have shown that tumor blood flow is highly heterogeneous in both clinical and experimental tumors.

Heterogeneous Perfusion Leads to Regions in the Tumor That Are Hypoxic and Acidic

Tumor hypoxia is so well recognized that numerous therapies have been developed to target hypoxic tissues (32–34). Hypoxia occurs in both clinical and experimental tumors, as measured by oxygen electrodes (35), electron paramagnetic resonance (EPR) (36), nuclear magnetic resonance (NMR) (37–41), single photon emission computed tomography (SPECT) (42), or positron emission tomography (PET; 43,44). Using ^{19}F MRI of hexafluorobenzene, Mason and colleagues have shown distinct heterogeneity in oxygenation of Dunning prostate carcinoma xenografts (38). In the clinical setting, an important technique for measurement of hypoxia is the use of N-1–substituted nitroimidazoles, which accumulate in hypoxic tissues. These compounds, usually misonidazole (MISO), are radiolabeled with positron emitters (e.g., ^{18}F) detected with PET. In a recent prospective study, Rasey's group has analyzed 37 preoperative patients with a variety of neoplasms and, using PET of ^{18}F MISO, found significant hypoxia in all but one patient (45). Hypoxic volumes ranged from 0% to 95% of the tumor, and there was significant heterogeneity between tumor types, within tumor groups, and between spatially distinct volumes of the same tumor. It should also be noted that MISO is only sensitive to extremely low levels of oxygen and that radiobiological resistance occurs at more modest levels of hypoxia (31,46). Thus, the clinically relevant hypoxic fraction may be greater than that estimated from MISO binding.

Hypoxia will lead to the overproduction of acid, because it induces the production of energy from glycolysis via the Pasteur effect. Moreover, a hallmark of many tumors is their ability to produce lactic acid, even in the presence of adequate oxygen (47). The low pH of tumors has been measured in clinical and experimental tumors by electrode (48) and by magnetic resonance spectroscopy (MRS) (Figure 3) (49–51). The increased glycolysis stimulated by the low oxygenation (52–55) will produce volumes lacking in both glucose and oxygen, and these tend to become necrotic (56).

Historically, tumor hypoxia was thought to be due to low capillary density, according to the model of Thomlinson and Gray (57). This model was based on the classic studies of August Krogh (58,59). In this model, capillaries supply oxygen to a cylinder (''Krogh cylinder'') of tissue that is

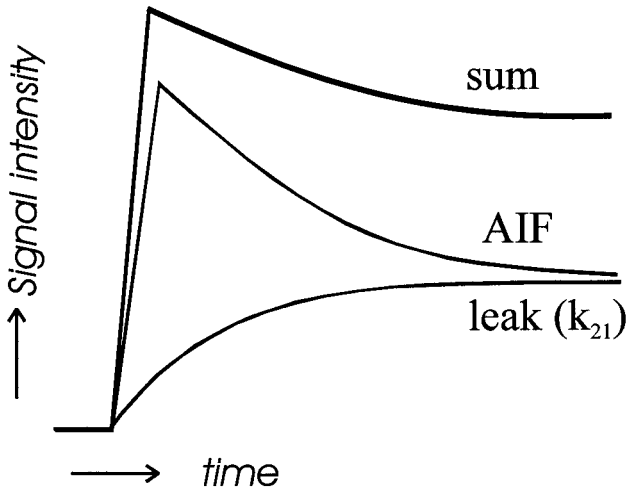

Figure 2. *Schematic of enhancement curve as a function of time in DEMRI. Sum refers to the signal observed in each voxel as a function of time. This signal has two major components: the arterial input function, which is related to the blood flow and the vascular volume, and the leak (k_{21}), which is related to the permeability and surface area of the blood vessels in each voxel.*

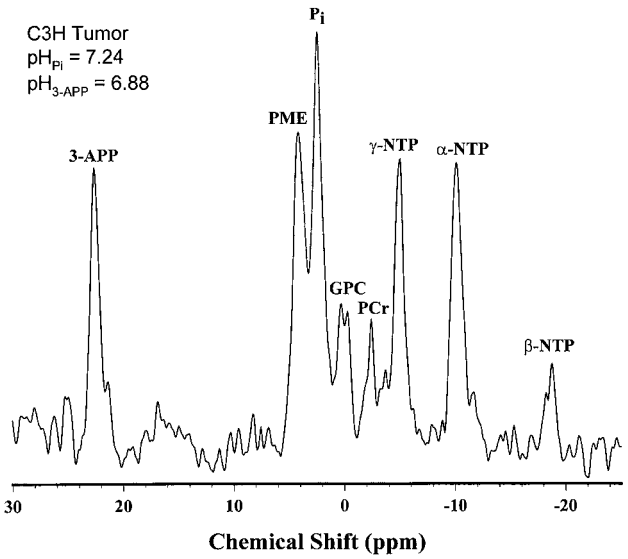

Figure 3. *PRESS-localized 31P-MR spectrum of a C3H tumor in the mammary fat pad of a C3H/Hen mouse. 3-aminopropylphosphonate (3-APP) is an exogenous, nontoxic, and impermeant indicator of the extracellular pH. (PME, phosphomonoesters; Pi, inorganic phosphate, primarily intracellular and used as indicator of intracellular pH; GPC, glycerolphosphorylcholine; PCr, phosphocreatine; NTP, nucleoside triphosphates).*

about 150 to 200 μm radius around the vessel. This distance is the limit of oxygen diffusion through respiring tissue, and is supported by studies with spheroids (60–63) as well as more recent polarographic measurements of oxygen in tumors (64). Although the classic Thomlinson and Gray model explains many aspects of tumor perfusion, it is inadequate because it does not take into account the time-variant aspects of blood flow and, more importantly, it assumes that all capillaries in the tumor are carrying oxygenated blood. This is likely not the case.

Hypoxia-Acidosis and Therapy

The existence of radioresistant hypoxic fractions is well established in rodent tumors and spontaneous human cancers. Oxygenated tumors and cells are three times more susceptible to radiation damage, compared with hypoxic/anoxic cells (65,66). The role of oxygen is to prolong the lifetime of ionized radicals generated by the interaction of radiation with macromolecules, as evidenced by the seminal observation that oxygen does not need to be present during irradiation but must be added within microseconds in order to sensitize (67). Oxygen is also required for emerging photodynamic therapies because many of these involve radical propagation (68,69).

Because the intracellular pH of cells in tumors remains neutral-to-alkaline (70), acidity of the interstitial space will increase resistance to many chemotherapies, based on a reduced partitioning of weakly basic chemotherapeutic drugs into the relatively alkaline cells. This occurs because of "ion trapping," wherein uncharged organic free bases are much more permeable than their protonated and charged counterparts and establish equal concentrations on both sides of the membrane. Because the ratio of charged-to-uncharged species increases with lower pH, more total base is found in acidic compartments (71–73). The partitioning of weak-base or weak-acid drug molecules across the plasma membrane of a tumor cell is dependent upon the acid-dissociation constant (pK_a) of the drug as well as the plasmalemmal pH gradient. A large acid-outside pH gradient can exert a protective effect upon the cell from weak-base drugs such as anthracyclines and vinca alkaloids, which have pK_a values of 7.5 to 9.5 (74–77). Recently, it has been shown that reversal of the tumor pH gradient with bicarbonate can improve the therapeutic efficacy of doxorubicin (pKa =7.6) (78), which is one of the most widely prescribed antineoplastic agents used in the treatment of breast cancer (79,80). Finally, hypoxia and acidity are indicative of poor perfusion. Poor perfusion itself provides a mechanical barrier to the delivery of drugs and hence produces a "physiological resistance" distinct from the effects of hypoxia or pH alone (2). Thus hypoxia and acidity are significant negative prognosticators for the efficacy of many anticancer therapies.

Hypoxia and Acidosis Promote Early and Late Aspects of Carcinogenesis

Hypoxia and acidosis promote early and late stages of carcinogenesis. For example, culturing of primary diploid Syrian hamster embryo cells at pH 6.7 induces them to spontaneously transform to a tumorigenic phenotype (81–83). This may occur because low pH is clastogenic, causing chromosomal strand breaks and rearrangements (84,85). Hypoxia is also clastogenic and mutagenic (86). At a later stage of carcinogenesis, low pH also induces invasive, migratory behavior *in vitro* (87) as well as metastasis *in vivo* (88), apparently through the activation and release of proteases (89–92). Hypoxia is also a potent inducer of metastatic behavior *in vitro* (92–94) and is a negative prognosticator for metastatic behavior *in vivo* (95,96). This is thought to occur via selection of cells that are resistant to hypoxia-induced, p53-dependent apoptosis (97). These data indicate that both hypoxia and acidosis promote the development of a more aggressive tumor phenotype.

Hypoxia and Acidosis Stimulate Angiogenesis

The acidic and hypoxic regions should also induce angiogenesis. Hypoxic induction of angiogenesis in tumor and normal tissues has been thoroughly and recently reviewed (98). Angiogenesis, or the growth of capillaries, is a necessary requirement for tumor growth (99–101). When cultured in a hypoxic environment, cells secrete active angiogenesis factors into the medium (102). The most generally important of these angiogenic factors in tumors is vascular endothelial growth factor (VEGF; also known as vascular permeability factor, VPF). VEGF is a complicated system because it exists in at least four isoforms, VEGF-A,-B,-C,-D, and VEGF-A is expressed in at least four

alternatively spliced forms, yielding products of 121, 165, 189, and 206 amino acids (103). VEGF-A-165 mRNA levels are dramatically increased within a few hours of exposing different cell cultures to hypoxia and return to background when normal oxygen supply is resumed (104). VEGF is also induced by glucose deprivation, stress, and hormones and is constitutively expressed in a number of tumor cell lines (105,106). Furthermore, receptors for VEGF are expressed on the endothelium of tumor vasculature, yet are virtually absent from vascular endothelium of adjoining tissue (107). Elegant studies using a tetracycline-regulated VEGF expression system (108) have shown that VEGF is important in inducing the growth and survival of new vessels but is not required to maintain mature vessels (109,110). The increased expression of VEGF is mediated through increased transcription, induced by hypoxia-inducible factor-1 (HIF-1), as well as increased VEGF mRNA stability (32,111). HIF-1 is a heterodimeric DNA binding complex composed of two basic helix-loop-helix PAS-proteins: HIF-1 beta/ARNT (aryl hydrocarbon receptor nuclear translocator), which is constitutively expressed, and HIF-1 alpha, which unstable in the presence of oxygen. At high levels of expression, HIF-1 promotes apoptosis, which may, in part, be responsible for cell loss in hypoxic/acidic regions of tumors (112). Although some cells have been reported to secrete VEGF in response to acidosis (113), this does not seem to be a general phenomenon in tumors.

Additional proangiogenic factors are induced by poor perfusion. For example, both hypoxia and low pH induce platelet-derived endothelial cell growth factor (PD-ECGF or thymidine phosphorylase) (114). There are data for hypoxic induction of basic fibroblast growth factor (FGF) in nontumor systems (115,116), and there is evidence to suggest that hypoxia and acidity modulate the interaction of this growth factor with the angiogenic network (117). Hypoxia also induces macrophage expression of acidic FGF and platelet-derived growth factor (PDGF), which are potent endothelial cell mitogens (116). A newly discovered family of angiogenesis regulators is angiopoietin-1 and –2, which act to differentiate and dedifferentiate the microvasculature, respectively (118,119). Current data suggest that hypoxia and VEGF interact with the angiopoietin system to dedifferentiate vasculature and prevent its maturation (120).

The observations that hypoxia and acidity are chronically present in tumors and that these parameters stimulate angiogenic growth factors raise an important question: Why are tumors not better perfused?

Poiseuille's Law and the Flow of Liquids in Tubes

In order to answer the question we have posed, the factors regulating blood flow must be considered. Jean Léonard Marie Poiseuille, the noted French engineer and physician, carried out extensive studies of the flow of water through cylindrical tubes. In 1846, he published a quantitative description of the relationship between flow rate (Q) of a viscous liquid through a capillary of diameter D, the pressure difference (ΔP) across the length (L) of the tube, and the viscosity of the liquid (η) (121). Poiseuille's law is stated mathematically by the equation:

$$Q = K \cdot \frac{\Delta P \cdot D^4}{L}$$

where the constant K is proportional to the reciprocal of the viscosity η. Later theoretical analyses (Hagenbach, 1860) led to the relationship now known as Poiseuille's law:

$$Q = \frac{\Delta P}{(8\eta L/\pi r^4)}$$

where ΔP is the pressure difference between two ends of the tube (i.e., the driving force), r is the radius of the tube, and the term ($8\eta L/\pi r^4$) represents the resistance to flow through the tube. Thus, flow resistance is proportional to the tube length and inversely proportional to the fourth power of tube diameter. This high sensitivity to diameter implies that vessel diameters must be tightly controlled to ensure adequate but not wasteful perfusion of tissue. The apparent viscosity η of blood varies with tube diameter in microvessels (122), but the fourth power dependence on tube diameter is the dominant effect.

Capillary Distribution and Tumor Perfusion

Tumor blood vessels have been described as chaotic, with larger than normal vessel diameters, longer vessel lengths (increased tortuosity), and high permeability. The local microvessel density (MVD) is also generally much more heterogeneous than that in normal tissues. All of these parameters can contribute to uneven blood distribution and hence, perfusion heterogeneity. Low perfusion in tumors can result from increased vessel length or tortuosity. Longer vessels result in a proportional increase in resistance and hence, a decrease in flow. The geometric flow resistance in neoplastic tissue can be two orders of magnitude higher than that observed in normal tissues (123,124). This increased resistance leads to decreased flow and hence would be expected to increase the residence time of erythrocytes in the capillary plexus. Indeed, erythrocyte velocity in tumor microvasculature can be an order of magnitude lower than in vessels of comparable diameter in normal tissue, especially at lower transcapillary pressures (125). However, in some tumor models, erythrocyte velocity is actually higher than normal (126,127). Thus, there is a wider distribution of blood flow in tumors compared with normal tissues. A similar heterogeneity can be seen when comparing local MVD with overall vascular density. Overall vascular density is rarely measured, yet in those cases in which it has been measured, it has been found to be less than that of normal tissues (128). In contrast, MVD in "hot spots" is often much higher than that seen in normal tissues, and the absolute MVD correlates strongly with tumor aggressiveness (129–131). It is hypothesized that the increased local MVD provides more avenues for

extravasation of tumor cells from the primary mass (132–135). Hence, although overall vascular density may be low, there are "hot spots" where the MVD is high, and these are heterogeneously distributed.

Regardless of the absolute number of vessels in a volume, the density must be related to the metabolic state of the tissue. Thus, even if the overall density were equal, a higher metabolic rate would lead to greater hypoxia. Recent models indicate that oxygen demand by cells is the most sensitive determinant of hypoxia in tissues (136,137). Because tumor cells generally have a higher metabolic demand than normal tissues, they require a more robust source of nutrients (3,52). The increased metabolic demand is likely related to proliferation. There is a clear requirement for microvasculature in the growth of tumors because tumors will not exceed more than approximately 2 mm in diameter without being vascularized (101). Furthermore, in a model system using implanted spheroids to mimic prevascularized tumor growth, it has been observed that, at an early stage, there is a net invasion of feeding vessels to the tumor, after which it begins to grow. However, the number and diameter of feeding vessels does not increase concomitant with the increase in tumor volume, indicating a mismatch between blood supply and metabolic demand (138). Dewhirst and coworkers have recently shown that such a limited arteriolar supply will contribute to longitudinal gradients that result in tumor hypoxia (139). Thus, there is a discontinuity between the overall vascular density of and the ability of the capillary plexus to provide tumors homogeneously and efficiently with oxygen and glucose required by metabolic demand.

Why Does Angiogenesis Not Reduce Acidosis and Hypoxia?

When the tumor as a whole is considered, an increase in vascular density *should* decrease resistance and increase blood flow, but this does not occur. This apparent contradiction likely arises from the evolution of regional heterogeneity during tumor growth and development. Pries and colleagues (140) have recently developed a model to describe how each segment of a microvascular network adjusts structurally in response to local stimuli and have compared these results with normal tissue (rat mesentery). They demonstrated that a minimal set of four types of adaptive responses is required to produce stable and realistic network structures (Table 1). The shear-dependent response causes enlargement of vessels carrying relatively large flow rates. The pressure-dependent response is responsible for the asymmetry of the vascular system, with arterioles smaller than corresponding venules. Responsiveness of local metabolic conditions, and the conduction of this information along upstream and downstream flow pathways, ensures that vessels experiencing unfavorable metabolic conditions (e.g., hypoxia and acidosis) receive increased blood flow.

Table 1. Adaptive Responses Necessary to Produce Functional and Efficient Vascular Networks.

• Response to wall shear stress
• Response to intravascular pressure
• Response to local metabolic conditions
• Conducted metabolic response

A considerable amount of evidence suggests that this finely balanced system is deranged in tumors. In particular, there is evidence that both the local response to metabolic conditions and the propagation of this response to upstream feeding vessels are impaired (141). The after paragraphs suggest possible mechanisms by which changes in the adaptive system lead to disturbances of vascular flow patterns as observed in tumors. It must be remembered that all the adaptive signals and responses are interrelated, so the actual mechanisms may be more complex than the simplified examples provided.

A number of angiogenic and antiangiogenic factors are important to the development of a mature and efficient vasculature. These include basic FGF, PDGF, nitric oxide, tumor necrosis factor-α, angiopoietins 1 and 2, and VEGF. At the risk of oversimplification, this discussion will be confined to VEGF as an example. VEGF can be constitutively secreted by tumor cells (142) while it is secreted by cells in normal tissues in response to stress (e.g., hypoxia, glucose deprivation) or hormonal stimulation (reviewed in Neeman (98)). This is illustrated in Figure 4, which shows capillary systems of normal and tumor tissues. In normal tissues, VEGF is secreted only by the hypoxic cells (blue) and not by the oxygenated cells (red), yielding a steep gradient of VEGF, which may be morphogenetic for new capillary growth. On the other hand, even well-oxygenated cells in tumors secrete some VEGF, so the gradient of VEGF is not as steep. The shallow gradient may cause dysmorphogenesis of the resulting neovasculature.

According to the model of Pries and colleagues (140), the propagated metabolic response is required to ensure that feeding vessels widen in response to increased demand for blood flow. This response may be reduced or absent in tumors, because the adaptive angiogenesis has not been reported to induce increased size or numbers of feeding vessels. Apparently, as tumors grow, feeding vessels do not adaptively respond to the increased demand, and the perfusion per unit volume drops across the entire tumor (139). Current knowledge regarding the behavior (i.e., diameter, number, pressure, and flow) of feeding vessels during tumor growth is lacking. However, microscopic observation of feeding vessels during growth of implanted spheroids indicates that they do not adaptively increase concomitant with the increase in tumor volume (M. Neeman, personal communication). Such conditions increase the requirement for a well-balanced blood distribution network.

Angiogenesis in response to local and conducted metabolic demands can occur in three ways, shown in Figure 5. In this figure, the initial condition is identical to that shown for tumors in Figure 4. In this diagram, each horizontal conduit represents a circuit of capillaries, the diameter of which is related to the inverse of resistance

across that circuit. Such circuits are called *modules* and do exist in normal tissues (143,144). Thus, the initial condition contains two parallel circuits, one with relatively high and the other with low resistance. Cells in the volume serviced by the high resistance circuit are hypoxic (blue). In response A, the conductive pathway increases the size of the afferent vessel (vertical vessel shown in red) and reduces the resistance across the lower capillary circuit. This results in evenly distributed blood flow and oxygenation of all cells. This is defined as *state I*, where increased angiogenesis increases tissue oxygenation, and is the state found in normal tissues (140). In response B, angiogenesis increases the diameter of the upper circuit, decreasing its resistance further. Consequently, more blood flows through this circuit and less through the lower, high resistance, circuit. Tissue in the region of the lower circuit becomes even more poorly oxygenated. This is termed *state II-P* because the decreased resistance of the upper circuit follows the addition of vasculature in parallel. In response C, angiogenesis increases the length of the lower circuit, causing a further increase in its resistance. As in response B, relatively more blood will pass through the upper circuit, and the tissues served by the lower circuit will become more hypoxic. This is termed *state II-S* because the increased resistance of the lower circuit occurred by addition of vasculature in series with existing vessels. Note that the poorly perfused (i.e., hypoxic-acidic) regions would be coincident with low MVD volumes in state II-P and with high MVD volumes in state II-S.

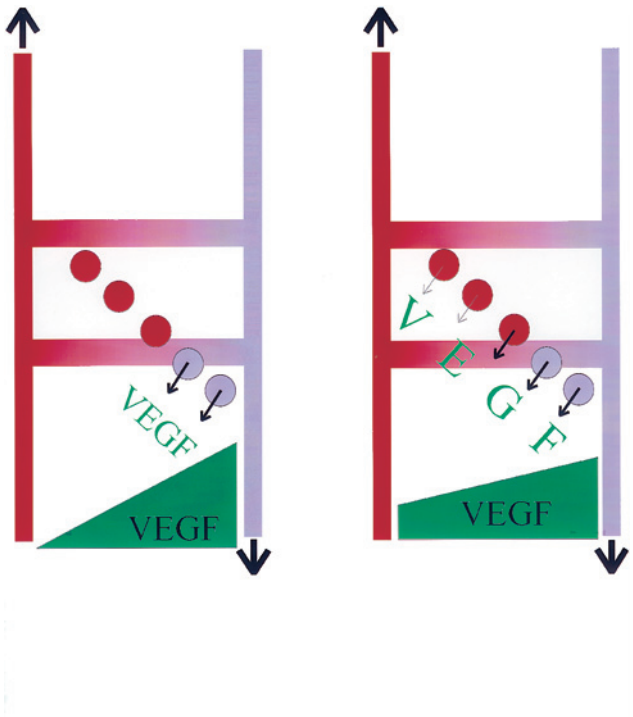

Figure 4. *Schematic showing differences in tumor and normal tissue vasculature. The vertical segments represent the afferent (red) and efferent (blue) vessels, and the cross members represent different capillary modules. The thickness of the capillary module is inversely proportional to the resistance. The color represents oxygenated (red) and deoxygenated (blue) blood. Cells are represented as circles and are either oxygenated (red) or deoxygenated (blue). In the normal tissues, only deoxygenated cells secrete VEGF, whereas all cells secrete VEGF in the tumor. The potential morphogenetic gradient for VEGF is shown in green and is steeper in the normal tissues.*

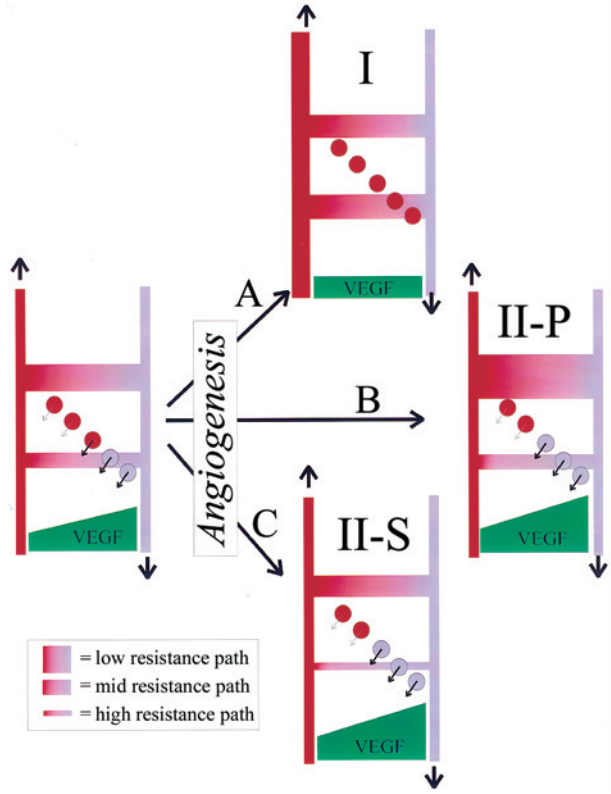

Figure 5. *The effect of angiogenesis on blood flow. In case A, angiogenesis results in a reduction of resistance across the lower module, which results in improved blood flow to this volume (state I). In case B, angiogenesis results in addition of new vessels in parallel with the upper module, causing a decrease in resistance, and this steals blood flow from the lower module, causing a volume of decreased perfusion. In case C, angiogenesis adds vessels in series with the lower module, causing an increase in resistance and reduced flow through this module.*

States I, II-P, and II-S are illustrated in more detail in Figure 6. State I shows balanced blood flow distribution. In state II-S, additional vessels are added in series and consequently increase resistance leading to lower blood flow in the upper module. In state II-P, vessels are added in parallel, decreasing the resistance and increasing the flow in the lower module. In Figure 6, the longitudinal gradient of hemoglobin oxygenation is shown as the transition from red to blue. As resistance decreases, flow rate increases, and consequently the residence time of erythrocytes in the capillary plexus goes down. Conversely, as resistance increases (relatively), the flow rate decreases, and the residence time goes up. In these regions of the capillary bed, the hemoglobin can be fully deoxygenated well before it exits the capillary plexus (29).

Evidence for Relatively Homogeneous Distribution of Flow in Normal Tissues

Ample evidence indicates that normal tissues are primarily in state I. In normal circulation, both intravascular and extra-

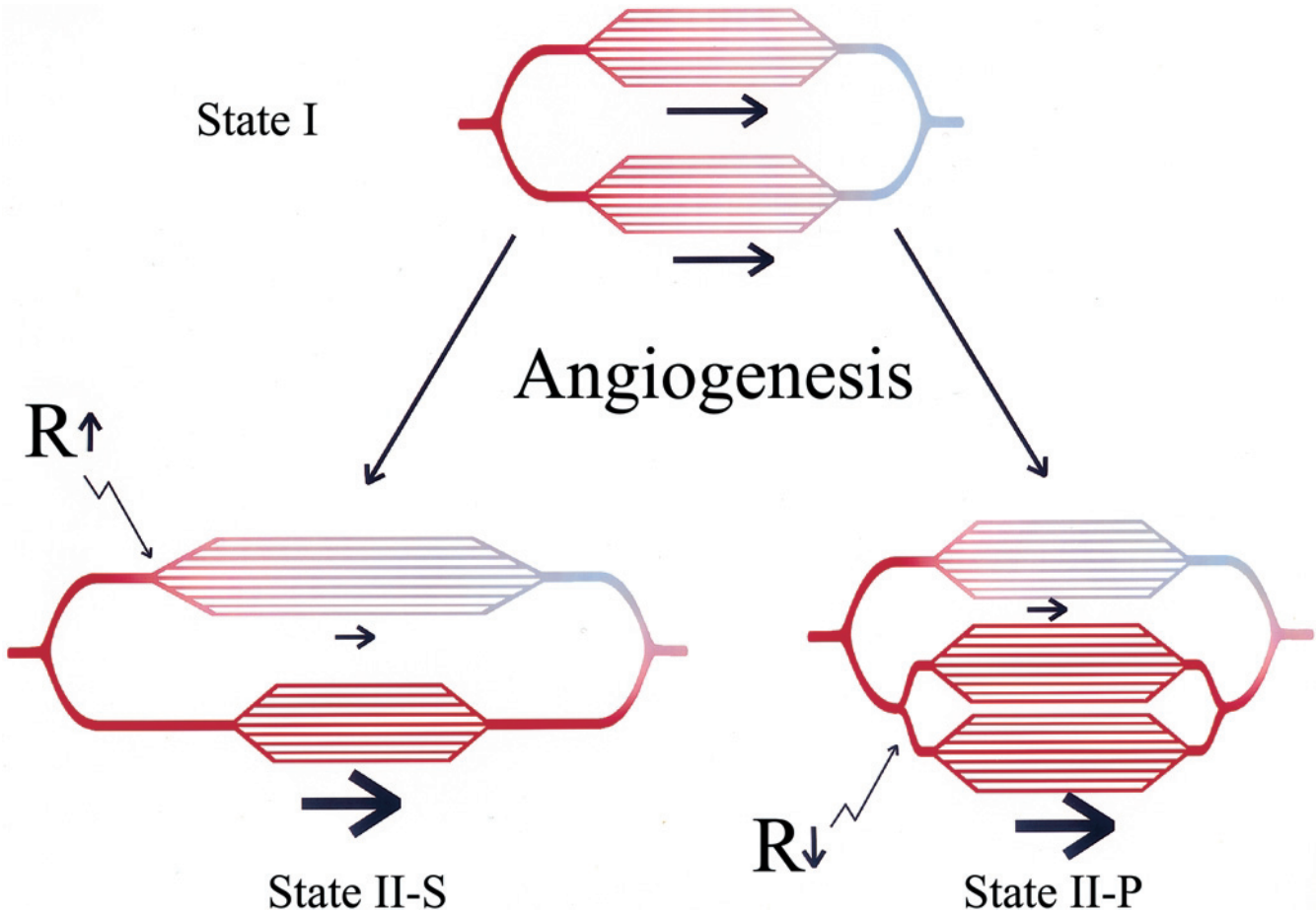

Figure 6. *Diagram showing angiogenesis in series and parallel. In the addition of vessels in series, the resistance increases, causing decreased flow through the upper module. In the addition of vessels in parallel, there is a decrease in the resistance, causing an increase in flow across the lower module. This steals flow from the upper module and causes decreased perfusion there.*

vascular P_{O_2} values decrease progressively from the large arterial vessels down to the small arterioles (145). Large arteries contain a blood P_{O_2} of about 100 mm Hg and smaller arterioles approximately 70 mm Hg oxygen. The concomitant drop in the transendothelial oxygen gradient is from 25 to 7.5 mm Hg. Thus, significant P_{O_2} gradients occur both longitudinally and radially in the arterial network. The longitudinal gradients represent losses of oxygen from precapillary vessels. At the organ level, these losses are even more severe (146). In skin, for instance, first-order arterioles (about 65 μm) have P_{O_2} levels of 50 mm Hg, whereas terminal arterioles (7–8 μm) have P_{O_2} values on the order of 35 mm Hg. The P_{O_2} in venules can be as high as 30 mm Hg (146).

The capillary system of hamster cremaster muscle has been extensively characterized by Sarelius and colleagues, with results corresponding to state I (147–149). First, there is a tight connection between metabolism and blood flow in microvessel networks such that increased flow is delivered to tissues with highest metabolic demand. Furthermore, there are predictable relationships between vessel length, pressure, and diameter. Finally, this entire network has been extensively modeled and shown to respond uniformly to downstream perturbations. A consequence of state I perfusion is that angiogenesis will improve tissue perfusion and this has been shown for normal tissues (150).

Evidence for Heterogeneous Flow Distribution in Tumor Tissues

There is much evidence that significant fractions of tumor tissues can exist in state II. For example, histological sections of clinical and experimental tumors often contain necrotic volumes, and these invariably contain vascular remnants (151). Clearly, the vasculature in this necrotic volume must not have provided sufficient perfusion, which is consistent with state II perfusion. Transcapillary resistance can be orders of magnitude higher in tumors than in normal tissues, which would be consistent with state II-S perfusion (123). Vascular branching patterns have been analyzed in a number of tumors and generally show an increased number of branches, compared with normal tissues. For example, Hori and colleagues have shown that terminal arterioles in transplanted hepatoma or lung carcinomas are on the order of 50 branches per 0.1 mm^2, compared to 14 per 0.1 mm^2 in normal tissues (152) , consistent with state II-P perfusion.

Additional evidence for the existence of state II perfusion in tumors includes the observations that antiangiogenic therapies, which reduce vessel density, also increase

susceptibility to chemotherapies (153–156). These observations suggest that the reduction of vasculature results in an improvement in perfusion and hence an improvement in therapeutic efficacy. Antiangiogenic therapies also potentiate the effectiveness of radiotherapy (157). These observations are consistent with the occurrence of state II perfusion in tumors.

More direct evidence for the presence of state II in tumors comes from MRI. In a comprehensive study of uterine cancers, Hawighorst and colleagues (158) compared DEMRI-measured parameters with histopathological markers, such as VEGF expression and MVD. Although volumes with high MVD correlated with volumes with high final signal gain, there was no correlation between MVD and the rate constant for signal increase. Thus, the volumes with high MVD will leak more contrast agent given enough time. Yet this will not occur rapidly, so MVD does not correlate with increased perfusion. This is clearly consistent with state II perfusion. Another important MRI observation for the existence of state II in tumors was made by Neeman and colleagues (159). Spheroids of VEGF-overexpressing C6 glioma cells were implanted in nude mice and the relative oxygenation was determined by the ratio of images collected before and after the administration of carbogen (95% oxygen, 5% carbon dioxide). Volumes with the highest vascular density exhibited the greatest signal increase in response to carbogen (160). Although open to discussion, one interpretation of this finding is that the volumes with the highest vascular density were the most hypoxic when the evaluation began.

Conclusions

Many studies have shown that tumors are heterogeneously perfused and that this represents a significant barrier to effective therapy. We reviewed these studies have and proposed that this heterogeneous perfusion arises from altered angiogenic responses to metabolic signals that normally regulate the structure of the blood distribution network. These abnormal responses may include addition of new microvessels in parallel to low resistance circuits and lengthening of existing microvessels in high resistance circuits. Additionally, arterioles feeding a tumor may not widen in response to decreased flow resistance in the regions that they supply because the conducted metabolic signal is diminished or absent. Hence, tumor growth and perfusion are ultimately limited by the architecture of the existing arteriolar network. This may lead to the extreme heterogeneity observed between individual tumors of the same type (161).

Acknowledgements

We thank J. Evelhoch, M. Dewhirst, Z. Bhujwalla, and M. Neeman for their helpful and insightful comments during the writing of this manuscript.

References

[1] Gullino PM (1980). Tumor pathophysiology: the perfusion model. *Antibiot Chemother* **28**, 35–42.

[2] Jain RK (1997). The Eugene M. Landis Award Lecture 1996. Delivery of molecular and cellular medicine to solid tumors. *Microcirculation* **4**, 1–23.

[3] Vaupel P, Kallinowski F, and Okunieff P (1990). Blood flow, oxygen consumption and tissue oxygenation of human tumors. *Adv Exp Med Biol* **277**, 895–905.

[4] Kidney DD, Dietrich RB, Goyal AK, Yan K, and Bradley WG, Jr. (1998). MRI of extracranial masses in children: the usefulness of gadolinium-chelate enhancement. *Pediatr Radiol* **28**, 322–328.

[5] Furman-Haran E, Grobgeld D, and Degani H (1997). Dynamic contrast-enhanced imaging and analysis at high spatial resolution of MCF7 human breast tumors. *J Magn Reson* **128**, 161–171.

[6] Tofts PS (1997). Modeling tracer kinetics in dynamic Gd-DTPA MR imaging. *J Magn Reson Imaging* **7**, 91–101.

[7] Hawighorst H, Knapstein PG, Weikel W, Knopp MV, Zuna I, Knof A, Brix G, Schaeffer U, Wilkens C, Schoenberg SO, Essig M, Vaupel P, and van Kaick G (1997). Angiogenesis of uterine cervical carcinoma: characterization by pharmacokinetic magnetic resonance parameters and histological microvessel density with correlation to lymphatic involvement. *Cancer Res* **57**, 4777–4786.

[8] Hawighorst H, Knopp MV, Debus J, Hoffmann U, Grandy M, Griebel J, Zuna I, Essig M, Schoenberg SO, DeVries A, Brix G, and van Kaick G (1998). Pharmacokinetic MRI for assessment of malignant glioma response to stereotactic radiotherapy: initial results. *J Magn Reson Imaging* **8**, 783–788.

[9] Su MY, Wang Z, Roth GM, Lao X, Samoszuk MK, and Nalcioglu O (1996). Pharmacokinetic changes induced by vasomodulators in kidneys, livers, muscles, and implanted tumors in rats as measured by dynamic Gd-DTPA-enhanced MRI. *Magn Reson Med* **36**, 868–877.

[10] Griebel J, Mayr NA, de Vries A, Knopp, MV, Gneiting T, Kremser C, Essig M, Hawighorst H, Lukas PH, and Yuh WT (1997). Assessment of tumor microcirculation: a new role of dynamic contrast MR imaging. *J Magn Reson Imaging* **7**, 111–119.

[11] Tofts PS, and Kermode AG (1991). Measurement of the blood-brain barrier permeability and leakage space using dynamic MR imaging. 1. Fundamental concepts. *Magn Reson Med* **17**, 357–367.

[12] Donahue KM, Weisskoff RM, and Burstein D (1997). Water diffusion and exchange as they influence contrast enhancement. *J Magn Reson Imaging* **7**, 102–110.

[13] Donahue KM, Weisskoff RM, Chesler DA, Kwong KK, Bogdanov, Jr AA, Mandeville JB, and Rosen BR (1996). Improving MR quantification of regional blood volume with intravascular T1 contrast agents: accuracy, precision, and water exchange. *Magn Reson Med* **36**, 858–867.

[14] Donahue KM, Weisskoff RM, Parmelee DJ, Callahan RJ, Wilkinson RA, Mandeville JB, and Rosen BR (1995). Dynamic Gd-DTPA enhanced MRI measurement of tissue cell volume fraction. *Magn Reson Med* **34**, 423–432.

[15] He ZQ, and Evelhoch JL (1998). Analysis of dynamic contrast enhanced MRI in tumors: relationship of derived parameters with physiologic factors. *Proc Int Soc Magn Reson Med* **6**, 1652.

[16] Reddick WE, Bhargava R, Taylor JS, Meyer WH, and Fletcher, BD (1995). Dynamic contrast-enhanced MR imaging evaluation of osteosarcoma response to neoadjuvant chemotherapy. *J Magn Reson Imaging* **5**, 689–694.

[17] Van Vierzen PB, Massuger LF, Ruys SH, and Barentsz JO (1998). Fast dynamic contrast enhanced MR imaging of cervical carcinoma. *Clin Radiol* **53**, 183–192.

[18] Barentsz JO, Berger-Hartog O, Witjes JA, Hulsbergen v, der KC, Oosterhof GO, VanderLaak JA, Kondacki H, and Ruijs SH (1998). Evaluation of chemotherapy in advanced urinary bladder cancer with fast dynamic contrast-enhanced MR imaging. *Radiology* **207**, 791–797.

[19] Barentsz JO, Jager GJ, Van Vierzen PB, Witjes JA, Strijk, SP, Peters H, Karssemeijer N, and Ruijs SH (1996). Staging urinary bladder cancer after transurethral biopsy: value of fast dynamic contrast-enhanced MR imaging. *Radiology* **201**, 185–193.

[20] Mayr NA, Yuh WT, Magnotta VA, Ehrhardt JC, Wheeler JA, Sorosky JI, Davis CS, Wen BC, Martin DD, Pelsang RE, Buller RE, Oberley, LW, Mellenberg DE, and Hussey DH (1996). Tumor perfusion studies using fast magnetic resonance imaging technique in advanced cervical cancer: a new noninvasive predictive assay. *Int J Radiat Oncol Biol Phys* **36**, 623–633.

[21] Mayr NA, Yuh WT, Zheng J, Ehrhardt JC, Magnotta VA, Sorosky JI, Pelsang RE, Oberley LW, and Hussey DH (1998). Prediction of tumor control in patients with cervical cancer: analysis of combined volume

and dynamic enhancement pattern by MR imaging. *Am J Roentgenol* **170**, 177–182.

[22] Bonnerot V, Charpentier A, Frouin F, Kalifa C, Vanel D, and Di Paola R (1992). Factor analysis of dynamic magnetic resonance imaging in predicting the response of osteosarcoma to chemotherapy. *Invest Radiol* **27**, 847–855.

[23] Vanel D, Di Paola R, and Contesso G (1987). Magnetic resonance imaging in musculoskeletal primary malignant tumors. *Magnetic Resonance Annual*, pp. 237–261.

[24] Acker JC, Dewhirst MW, Honore GM, Samulski TV, Tucker, JA, and Oleson JR (1990). Blood perfusion measurements in human tumours, evaluation of laser Doppler methods. *Int J Hypertherm* **6**, 287–304.

[25] Vaupel P (1998). Tumor blood flow. In Blood Perfusion And Microenvironment Of Human Tumors: Implications For Clinical Radio-Oncology. M Molls and P Vaupel, Eds. Springer-Verlag, Berlin. pp. 41–46.

[26] Algire GH (1943). Transplantable tumors grown in transparent chambers in skinflaps of mice. *J Natl Cancer Inst* **4**, 1–8.

[27] Dudar TE, and Jain RK (1984). Differential response of normal and tumor microcirculation to hyperthermia. *Cancer Res* **44**, 605–612.

[28] Dewhirst MW, Gustafson C, Gross JF, and Tso CY (1987). Temporal effects of 5.0 Gy radiation in healing subcutaneous microvasculature of a dorsal flap window chamber. *Radiation Research* **112**, 581–591.

[29] Dewhirst MW (1998). Concepts of oxygen transport at the microcirculatory level. *Semin Rad Oncol* **8**, 143–150.

[30] Dewhirst MW, Braun RD, and Lanzen JL (1998). Temporal changes in PO2 of R3230AC tumors in Fischer-344 rats. *Int J Radiat Oncol Biol Phys* **42**, 723–726.

[31] Kimura H, Braun RD, Ong ET, Hsu R, Secomb TW, Papahadjopoulos D, Hong, and Dewhirst MW (1996). Fluctuations in red cell flux in tumor microvessels can lead to transient hypoxia and reoxygenation in tumor parenchyma. *Cancer Res* **56**, 5522–5528.

[32] Blancher C, and Harris AL (1998). The molecular basis of the hypoxia response pathway: tumour hypoxia as a therapy target. *Cancer Metastasis Rev* **17**, 187–194.

[33] Biaglow JE, Manevich Y, Leeper D, Chance B, Dewhirst MW, Jenkins WT, Tuttle SW, Wroblewski K, Glickson JD, Stevens C, and Evans SM (1998). MIBG inhibits respiration: potential for radio- and hyperthermic sensitization. *Int J Radiat Oncol Biol Phys* **42**, 871–876.

[34] Dewhirst MW, Ozimek EJ, Gross J, and Cetas TC (1980). Will hyperthermia conquer the elusive hypoxic cell? Implications of heat effects on tumor and normal-tissue microcirculation. *Radiology* **137**, 811–817.

[35] Nozue M, Lee I, Yuan F, Teicher BA, Brizel DM, Dewhirst, MW, Milross CG, Milas L, Song CW, Thomas CD, Guichard M, Evans SM, Koch CJ, Lord EM, Jain RK, and Suit HD (1997). Interlaboratory variation in oxygen tension measurement by Eppendorf "Histograph" and comparison with hypoxic marker. *J Surg Oncol* **66**, 30–38.

[36] Halpern HJ, Yu C, Peric M, Barth ED, Karczmar GS, River, JN, Grdina DJ, and Teicher BA (1996). Measurement of differences in pO2 in response to perfluorocarbon/carbogen in FSa and NFSa murine fibrosarcomas with low-frequency electron paramagnetic resonance oximetry. *Radiat Res* **145**, 610–618.

[37] Hasegawa Y, Formato JE, Latour LL, Gutierrez JA, Liu KF, Garcia JH, Sotak CH, and Fisher M (1996). Severe transient hypoglycemia causes reversible change in the apparent diffusion coefficient of water. *Stroke* **27**, 1648–1655.

[38] Mason RP, Hunjan S, Le D, Constantinescu A, Barker BR, Wong PS, Peschke P, Hahn EW, and Antich PP (1998). Regional tumor oxygen tension: fluorine echo planar imaging of hexafluorobenzene reveals heterogeneity of dynamics. *Int J Radiat Oncol Biol Phys* **42**, 747–750.

[39] Mason RP, Rodbumrung W, and Antich PP (1996). Hexafluorobenzene: a sensitive 19F NMR indicator of tumor oxygenation. *NMR Biomed* **9**, 125–134.

[40] Al-Hallaq HA, River JN, Zamora M, Oikawa H, and Karczmar GS (1998). Correlation of magnetic resonance and oxygen microelectrode measurements of carbogen-induced changes in tumor oxygenation. *Int J Radiat Oncol Biol Phys* **41**, 151–159.

[41] Oikawa H, Al-Hallaq HA, Lewis MZ, River JN, Kovar DA, and Karczmar GS (1997). Spectroscopic imaging of the water resonance with short repetition time to study tumor response to hyperoxia. *Magn Reson Med* **38**, 27–32.

[42] Wiebe LI, and Stypinski D (1996). Pharmacokinetics of SPECT radiopharmaceuticals for imaging hypoxic tissues. *Q J Nucl Med* **40**, 270–284.

[43] Koh WJ, Rasey JS, Evans ML, Grierson JR, Lewellen TK, Graham MM, Krohn, KA, and Griffin TW (1992). Imaging of hypoxia in human tumors with (F-18)fluoromisonidazole. *Int J Radiat Oncol Biol Phys* **22**, 199–212.

[44] Kavanagh MC, Sun A, Hu Q, and Hill RP (1996). Comparing techniques of measuring tumor hypoxia in different murine tumors: Eppendorf pO2 Histograph, (3H)misonidazole binding and paired survival assay. *Radiat Res* **145**, 491–500.

[45] Rasey JS, Koh WJ, Evans ML, Peterson LM, Lewellen TK, Graham MM, and Krohn KA (1996). Quantifying regional hypoxia in human tumors with positron emission tomography of (18F)fluoromisonidazole: a pretherapy study of 37 patients. *Int J Radiat Oncol Biol Phys* **36**, 417–428.

[46] Wouters BG, and Brown JM (1997). Cells at intermediate oxygen levels can be more important that the "hypoxic fraction" in determining tumor response to fractionated radiotherapy. *Radiat Res* **147**, 541–550.

[47] Warburg O (1956). On the origin of cancer cells. *Science* **123**, 309–314.

[48] Wike-Hooley JL, Haveman J, and Reinhold HS (1984). The relevance of tumour pH to the treatment of malignant disease. *Radiother Oncol* **2**, 343–366.

[49] Gillies RJ, Liu Z, and Bhujwalla ZM (1994). ^{31}P-MRS measurements of extracellular pH of tumors using 3-aminopropylphosphonate. *Am J Physiol* **267**, C195–C203.

[50] McCoy CL, Parkins CS, Chaplin DJ, Griffiths JR, Rodrigues LM, and Stubbs M (1995). The effect of blood flow modification on ontra- and extracellular pH measured by 31P magnetic resonance spectroscopy in murine tumours. *Br J Cancer* **72**, 905–911.

[51] Stubbs M, Robinson SP, Rodrigues LM, Parkins CS, and Griffiths JR (1995). Cellular ion homeostasis in Morris hepatoma 9618a *in vivo* after host carbogen (95% O_2/ 5% CO_2) breathing. *Proc Int Soc Magn Reson Med* **3**, 1093.

[52] Gullino PM (1976). *In vivo* utilization of oxygen and glucose by neoplastic tissue. *Adv Exp Med Biol* **75**, 521–536.

[53] Gullino PM, Grantham FH, and Courtney AH (1967). Glucose consumption by transplanted tumors *in vivo*. *Cancer Res* **27**, 1031–1040.

[54] Gullino PM, Grantham FH, and Courtney AH (1967). Utilization of oxygen by transplanted tumors *in vivo*. *Cancer Res* **27**, 1020–1030.

[55] Gullino PM, Grantham FH, Courtney AH, and Losonczy I (1967). Relationship between oxygen and glucose consumption by transplanted tumors *in vivo*. *Cancer Res* **27**, 1041–1052.

[56] Freyer JP, and Sutherland RM (1986). Proliferative and clonogenic heterogeneity of cells from EMT6/Ro multicellular spheroids induced by the glucose and oxygen supply. *Cancer Res* **46**, 3513–3520.

[57] ThomLinson RH, and Gray LH (1955). The histological structure of some human lung cancers and the possible implications for radiotherapy. *Br J Cancer* **9**, 539–549.

[58] Krogh A (1919). The rate of diffusion of gases through animal tissues, with some remarks on the coefficient of invasion. *J Physiol* **52**, 391–408.

[59] Krogh A (1919). The number and distribution of capillaries in muscles with calculations of the oxygen pressure head necessary for supplying the tissue. *J Physiol* **52**, 409–415.

[60] Freyer JP, and Sutherland RM (1985). A reduction in the *in situ* of oxygen and glucose consumption of cells in EMT6/RO spheroids during growth. *J Cell Physiol* **125**, 516–524.

[61] Freyer JP, and Sutherland RM (1983). Determination of diffusion constants for metabolites in multicell tumor spheroids. *Oxygen Transport to Tissue IV. Adv. Exp. Med. Biol.* **159**, 43–47

[62] Neeman M, Jarrett KA, Sillerud LO, and Freyer JP (1991). Self-diffusion of water in multicellular spheroids measured by magnetic resonance microimaging. *Cancer Res* **51**, 4072–4079.

[63] Sillerud LO, Freyer JP, Neeman M, and Mattingly MA (1990). Proton NMR microscopy of multicellular tumor spheroid morphology. *Magn Reson Med* **16**, 380–389.

[64] HelmLinger G, Yuan F, Jain MD, and Jain R (1997). Interstitial pH and pO_2 Gradients in Solid Tumors *in vivo*: High-Resolution Measurements Reveal a Lack of Correlation. *Nature Med* **3**, 177–182.

[65] Hall EJ (1994). Radiobiology for the Radiologist. J.B. Lippincott, Philadelphia.

[66] Parliament MB, Chapman JD, Urtasun RC, McEwan AJ, Golberg L, Mercer JR, Mannan RH, and Wiebe LI (1992). Non-invasive assessment of human tumour hypoxia with 123I-iodoazomycin arabinoside: preliminary report of a clinical study. *Br J Cancer* **65**, 90–95.

[67] Michael B, Adams G, Hewitt H, Jones W, and Watts M (1973). A posteffect of oxygen in irradiated bacteria: A submillisecond fast mixing study. *Radiat Res* **54**, 239–251.
[68] Freitas I (1985). Role of hypoxia in photodynamic therapy of tumors. *Tumori* **71**, 251–259.
[69] Yuan J, Mahama-Relue PA, Fournier RL, and Hampton JA (1997). Predictions of mathematical models of tissue oxygenation and generation of singlet oxygen during photodynamic therapy. *Radiat Res* **148**, 386–394.
[70] Griffiths JR (1991). Are cancer cells acidic? *Br J Cancer* **64**, 425–427.
[71] Gillies RJ, and Deamer DW (1978). Intracellular pH: Methods and applications. *Curr Top Bioenergetics* **9**, 63–87.
[72] Roos A (1978). Weak acids, weak bases and intracellular pH. *Respir Physiol* **33**, 27–30.
[73] Raghunand R, Martinez-Zaguilan R, Wright SH, and Gillies RJ (1999). pH and Drug Resistance II. Turnover of acidic vesicles and resistance to weakly basic chemotherapeutic drugs. *Biochem Pharmacol* **57**, 1047–1058.
[74] Tannock IF, and Rotin D (1989). Acid pH in Tumors and Its Potential for Therapeutic Exploitation. *Cancer Res* **49**, 4373–4384.
[75] Roepe PD, Wei LY, Cruz J, and Carlson D (1993). Lower electrical membrane potential and altered pHi homeostasis in multidrug-resistant (MDR) cells: further characterization of a series of MDR cell lines expressing different levels of p-glycoprotein. *Biochemistry* **32**, 11042–11056.
[76] Simon S, Roy D, and Schindler M (1994). Intracellular pH and the control of multidrug resistance. *Cell Biol* **91**, 1128–1132.
[77] Gerweck L, and Seetharaman K (1996). Cellular pH gradient in tumor versus normal tissue: Potential for exploitation for the treatment of cancer. *Cancer Res* **56**, 1194–1198.
[78] Raghunand N, He X, van Sluis R, Mahoney B, Baggett B, Taylor CW, Paine-Murrieta G, Roe D, Bhujwalla ZM, and Gillies RJ (1999). Enhancement of chemotherapy by manipulation of tumor pH. *Br J Cancer* **80**, 1011.
[79] Taylor CW, Dalton WS, Parrish PR, Gleason MC, Bellamy WT, Thompson FH, Roe DJ, and Trent JM (1991). Different mechanisms of decreased drug accumulation in doxorubicin and mitoxantrone resistant variants of the MCF7 human breast cancer cell line. *Br J Cancer* **63**, 923–929.
[80] Simon SM, and Schindler M (1994). Cell biological mechanisms of multidrug resistance in tumors. *Proc Nat Acad Sci USA* **91**, 3497–3504.
[81] LeBoeuf RA, and Kerckaert GA (1987). Enhanced morphological transformation of early passage syrian hamster embryo cells cultured in medium with a reduced bicarbonate concentration and pH. *Carcinogenesis* **8**, 689–697.
[82] LeBoeuf RA, Kerckaert GA, Aardema MJ, Poiley JA, and Raineri R (1990). Enhanced morphological and neoplastic transformation of syrian hamster embryo cells cultured at pH 6.70. *Mutat Environment* **D**, 219–228.
[83] LeBoeuf RA, Kerckaert GA, Poiley JA, and Raineri R (1989). An interlaboratory comparison of enhanced morphological transformation of syrian hamster embryo cells cultured under conditions of reduced bicarbonate concentration and pH. *Mutat Res* **222**, 205–218.
[84] Morita T, Nagaki T, Fukuda I, and Okumura K (1992). Clastogenicity of low pH to various cultured mammalian cells. *Mutat Res* **268**, 297–305.
[85] Morita T, Takeda K, and Okumura K (1990). Evaluation of clastogenicity of formic acid, acetic acid, and lactic acid on cultured mammalian cells. *Mutat Res* **240**, 195–202.
[86] Reynolds TY, Rockwell S, and Glazer PM (1996). Genetic instability induced by the tumor microenvironment. *Cancer Res* **56**, 5754–5757.
[87] Martinez-Zaguilan R, Seftor EA, Seftor REB, Chu YW, Gillies RJ, and Hendrix MJC (1996). Acidic pH Enhances The Invasive Behavior of Human Melanoma Cells. *Clin. Exp Metastasis* **14**, 176–186.
[88] Schlappack OK, Zimmermann A, and Hill RP (1991). Glucose starvation and acidosis: effect on experimental metastasic potential, DNA content and MTX resistance of murine tumour cells. *Br J Cancer* **64**, 663–670.
[89] Montcourrier P, Silver I, Farnoud R, Bird I, and Rochefort H (1997). Breast Cancer Cells Have a High Capacity To Acidify Extracellular Milieu by a Dual Mechanism. *Clin Exp Metastasis* **15**, 382–392.
[90] Rozhin J, Sameni M, Ziegler G, and Sloane BF (1994). Pericellular pH affects distribution and secretion of cathepsin B in Malignant Cells. *Cancer Res* **54**, 6517–6525.
[91] Cuvier C, Jang A, and Hill RP (1997). Exposure to hypoxia, glucose starvation and acidosis: effect on invasive capacity of murine tumor cells and correlation with cathepsin (L + B) secretion. *Clin Exp Metastasis* **15**, 19–25.
[92] Jang A, and Hill RP (1997). An examination of the effects of hypoxia, acidosis, and glucose starvation on the expression of metastasis-associated genes in murine tumor cells. *Clin Exp Metastasis* **15**, 469–483.
[93] Graham CH, Forsdike J, Fitzgerald CJ, and Macdonald-Goodfellow S (1999). Hypoxia-mediated stimulation of carcinoma cell invasiveness via upregulation of urokinase receptor expression. *Int J Cancer* **80**, 617–623.
[94] Fitzpatrick TE, and Graham CH (1998). Stimulation of plasminogen activator inhibitor-1 expression in immortalized human trophoblast cells cultured under low levels of oxygen. *Exp CellRes* **245**, 155–162.
[95] Brizel DM, Scully SP, Harrelson JM, Layfield LJ, Bean JM, Prosnitz LR, and Dewhirst MW (1996). Tumor oxygenation predicts for the likelihood of distant metastases in human soft tissue sarcoma. *Cancer Res* **56**, 941–943.
[96] Sundfor K, Lyng H, and Rofstad EK (1998). Tumour hypoxia and vascular density as predictors of metastasis in squamous cell carcinoma of the uterine cervix. *Br J Cancer* **78**, 822–827.
[97] Kim CY, Tsai MH, Osmanian C, Graeber TG, Lee JE, Giffard RG, DiPaolo JA, Peehl DM, and Giaccia AJ (1997). Selection of human cervical epithelial cells that possess reduced apoptotic potential to low-oxygen conditions. *Cancer Res* **57**, 4200–4204.
[98] Neeman M, Abramovitch R, Schiffenbauer YS, and Tempel C (1997). Regulation of angiogenesis by hypoxic stress: from solid tumours to the ovarian follicle. *Int J Exp Pathol* **78**, 57–70.
[99] Gullino PM (1983). Angiogenesis and neoplastic growth. *Prog Clin Biol Res* **132C**, 101–107.
[100] Gullino PM (1978). Angiogenesis and oncogenesis. *J Natl Cancer Inst* **61**, 639–643.
[101] Hanahan D, and Folkman J (1996). Patterns and emerging mechanisms of the angiogenic switch during tumorigenesis. *Cell* **86**, 353–364.
[102] Knighton DR, Hunt TK, Scheuenstuhl H, Halliday BJ, Werb, and Banda MJ (1983). Oxygen tension regulates the expression of angiogenesis factor by macrophages. *Science* **221**, 1283–1285.
[103] Scott PA, Gleadle JM, Bicknell R, and Harris AL (1998). Role of the hypoxia sensing system, acidity and reproductive hormones in the variability of vascular endothelial growth factor induction in human breast carcinoma cell lines. *Int J Cancer* **75**, 706–712.
[104] Shweiki D, Itin A, Soffer D, and Keshet E (1992). Vascular endothelial growth factor induced by hypoxia may mediate hypoxia-initiated angiogenesis. *Nature* **359**, 843–845.
[105] Shweiki D, Neeman M, Itin A, and Keshet E (1995). Induction of vascular endothelial growth factor expression by hypoxia and by glucose deficiency in multicell spheroids: implications for tumor angiogenesis. *Proc Nat Acad Sci USA* **92**, 768–772.
[106] Potgens AJ, Lubsen NH, van Altena MC, Schoenmakers JG, Ruiter DJ, and de Waal RM (1995). Vascular permeability factor expression influences tumor angiogenesis in human melanoma lines xenografted to nude mice. *Am J Pathol* **146**, 197–209.
[107] Olson TA, Mohanraj D, Roy S, and Ramakrishnan S (1997). Targeting the tumor vasculature: inhibition of tumor growth by a vascular endothelial growth factor-toxin conjugate. *Int J Cancer* **73**, 865–870.
[108] Benjamin LE, and Keshet E (1996). Conditional switching of vascular endothelial growth factor (VEGF) expression in tumors: induction of endothelial cell shedding and regression of hemangioblastoma-like vessels by VEGF withdrawal. *Proc Nat Acad Sci USA* **94**, 8761–8766.
[109] Benjamin LE, Golijanin D, Itin A, Pode D, and Keshet E (1999). Selective ablation of immature blood vessels in established human tumors follows vascular endothelial growth factor withdrawal. *J Clin Invest* **103**, 159–165.
[110] Yu C, Harris SR, and Thorgeirsson UP (1997). Vascular endothelial growth factor is essential for initial but not continued *in vivo* growth of human breast carcinoma cells. *Cancer Res* **57**, 3924–3928.
[111] Stein I, Neeman M, Shweiki D, Itin A, and Keshet E (1995). Stabilization of vascular endothelial growth factor mRNA by hypoxia and hypoglycemia and coregulation with other ischemia-induced genes. *Mol Cell Biol* **15**, 5363–5368.
[112] Carmeliet P, Dor Y, Herbert JM, Fukumura D, Brusselmans K, Dewerchin M, Neeman M, Bono F, Abramovitch R, Maxwell P, Koch CJ, Ratcliffe P, Moons L, Jain RK, Collen D, and Keshet E (1998). Role of HIF-1alpha in hypoxia-mediated apoptosis, cell proliferation and tumour angiogenesis. *Nature* **394**, 485–490.
[113] Brooks SE, Gu X, Kaufmann PM, Marcus DM, and Caldwell RB (1998). Modulation of VEGF production by pH and glucose in retinal Muller cells. *Curr Eye Res* **17**, 875–882.

[114] Griffiths L, Dachs GU, Bicknell R, Harris AL, and Stratford IJ (1997). The influence of oxygen tension and pH on the expression of platelet-derived endothelial cell growth factor/thymidine phosphorylase in human breast tumor cells grown *in vitro* and *in vivo*. *Cancer Res* **57**, 570–572.

[115] Phillips PG, Birnby LM, and Narendran A (1995). Hypoxia induces capillary network formation in cultured bovine pulmonary microvessel endothelial cells. *Am J Physiol* **268**, L789–L800.

[116] Kuwabara K, Ogawa S, Matsumoto M, Koga S, Clauss M, Pinsky DJ, Lyn P, Leavy J, Witte L, and Joseph-Silverstein J (1995). Hypoxia-mediated induction of acidic/basic fibroblast growth factor and platelet-derived growth factor in mononuclear phagocytes stimulates growth of hypoxic endothelial cells. *Proc Nat Acad Sci USA* **92**, 4606–4610.

[117] Kumar R, Kuniyasu H, Bucana CD, Wilson MR, and Fidler IJ (1998). Spatial and temporal expression of angiogenic molecules during tumor growth and progression. *Oncol Res* **10**, 301–311.

[118] Davis S, and Yancopoulos GD (1999). The angiopoietins: Yin and Yang in angiogenesis. *Curr Top Microbiol Immunol* **237**, 173–185.

[119] Davis S, Aldrich TH, Jones PF, Acheson A, Compton DL, Jain V, Ryan TE, Bruno J, Radziejewski C, Maisonpierre PC, and Yancopoulos GD (1996). Isolation of angiopoietin-1, a ligand for the TIE2 receptor, by secretion-trap expression cloning. *Cell* **87**, 1161–1169.

[120] Mandriota SJ, and Pepper MS (1998). Regulation of angiopoietin-2 mRNA levels in bovine microvascular endothelial cells by cytokines and hypoxia. *Circ Res* **83**, 852–859.

[121] Poiseuille J (1846). Recherches expérimentales sur le mouvement des liquides dans les tubes de très petits diamètres. *Mém Savant Étrangers Paris* **9**, 433–544.

[122] Pries AR, Secomb T, Gessner T, Sperandio MB, Gross J, and Gaehtgens P (1994). Resistance to blood flow in microvessels *in vivo*. *Circ Res* **75**, 904–915.

[123] Less JR, Posner MC, Skalak TC, Wolmark N, and Jain RK (1997). Geometric resistance and microvascular network architecture of human colorectal carcinoma. *Microcirculation* **4**, 25–33.

[124] Wu NZ, Da D, Rudoll TL, Needham D, Whorton AR, and Dewhirst, MW (1993). Increased microvascular permeability contributes to preferential accumulation of Stealth liposomes in tumor tissue. *Cancer Res* **53**, 3765–3770.

[125] Jain RK (1996). 1995 Whitaker Lecture: delivery of molecules, particles, and cells to solid tumors. *Ann Biomed Eng* **24**, 457–473.

[126] Dewhirst MW, Tso CY, Oliver R, Gustafson CS, Secomb TW, and Gross JF (1989). Morphologic and hemodynamic comparison of tumor and healing normal tissue microvasculature. *Int J Radiat Oncol Biol Phys* **17**, 91–99.

[127] Brizel DM, Klitzman B, Cook JM, Edwards J, Rosner G, and Dewhirst MW (1993). A comparison of tumor and normal tissue microvascular hematocrits and red cell fluxes in a rat window chamber model. *Int J Radiat Oncol Biol Phys* **25**, 269–276.

[128] Foltz RM, McLendon RE, Friedman HS, Dodge RK, Bigner DD, and Dewhirst MW (1995). A pial window model for the intracranial study of human glioma microvascular function. *Neurosurgery* **36**, 976–984.

[129] Bevilacqua P, Barbareschi M, Verderio P, Boracchi P, Caffo O, Dalla, Palma P, Meli S, Weidner N, and Gasparini G (1995). Prognostic value of intratumoral microvessel density, a measure of tumor angiogenesis, in node-negative breast carcinoma–results of a multi-parametric study. *Breast Cancer Res Treat* **36**, 205–217.

[130] Weidner N (1995). Current pathologic methods for measuring intratumoral microvessel density within breast carcinoma and other solid tumors. *Breast Cancer Res Treat* **36**, 169–180.

[131] Weidner N (1995). Intratumor microvessel density as a prognostic factor in cancer. *Am J Path* **147**, 9–19.

[132] Ziche M, and Gullino PM (1982). Angiogenesis and neoplastic progression *in vitro*. *J Natl Cancer Inst* **69**, 483–487.

[133] Brem SS, Jensen HM, and Gullino PM (1978). Angiogenesis as a marker of preneoplastic lesions of the human breast. *Cancer* **41**, 239–244.

[134] Weidner N, and Folkman J (1996). Tumoral vascularity as a prognostic factor in cancer. *Important Adv Oncol* 167–190.

[135] Teicher BA (1995). Angiogenesis and cancer metastases: therapeutic approaches. *Crit Rev Oncol Hematol* **20**, 9–39.

[136] Secomb TW, Hsu R, Ong ET, Gross JF, and Dewhirst MW (1995). Analysis of the effects of oxygen supply and demand on hypoxic fraction in tumors. *Acta Oncol* **34**, 313–316.

[137] Secomb TW, Hsu R, Braun RD, Ross JR, Gross JF, and Dewhirst, MW (1998). Theoretical simulation of oxygen transport to tumors by three-dimensional networks of microvessels. *Adv Exp Med Biol* **454**, 629–634.

[138] Abramovitch R, Meir G, and Neeman M (1995). Neovascularization induced growth of implanted C6 glioma multicellular spheroids: magnetic resonance microimaging. *Cancer Res* **55**, 1956–1962.

[139] Dewhirst MW, Ong ET, Braun RD, Smith B, Klitzman B, Evans SM, and Wilson D (1999). Quantification of longitudinal tissue pO_2 gradients in window chamber tumours: impact on tumour hypoxia. *Br J Cancer* **79**, 1717–1722.

[140] Pries AR, Secomb T, and Gaehtgens P (1998). Structural adaptation and stability of microvascular networks: theory and simulations. *Am J Physiol* **275**, H349–H360.

[141] Gulledge CJ, and Dewhirst MW (1996). Tumor oxygenation: a matter of supply and demand. *Anticancer Res* **16**, 741–749.

[142] Scott PA, Gleadle JM, Bicknell R, and Harris AL (1998). Role of the hypoxia sensing system, acidity and reproductive hormones in the variability of vascular endothelial growth factor induction in human breast carcinoma cell lines. *Int J Cancer* **75**, 706–712.

[143] Berg BR, and Sarelius IH (1996). Erythrocyte flux in capillary networks during maturation: implications for oxygen delivery. *Am J Physiol* **271**, H2263–H2273.

[144] Sweeney TE, and Sarelius IH (1989). Arteriolar control of capillary cell flow in striated muscle. *Circ Res* **64**, 112–120.

[145] Duling BR, Kuschinsky W, and Wahl M (1979). Measurements of the perivascular PO2 in the vicinity of the pial vessels of the cat. *Pflugers Arch* **383**, 29–34

[146] Torres FI, Kerger H, and Intaglietta M (1996). pO2 measurements in arteriolar networks. *Microvasc Res* **51**, 202–212.

[147] Berg BR, and Sarelius IH (1995). Functional capillary organization in striated muscle. *Am J Physiol* **268**, H1215–H1222.

[148] Kiani MF, Cokelet GR, and Sarelius IH (1993). Effect of diameter variability along a microvessel segment on pressure drop. *Microvasc Res* **45**, 219–232.

[149] Kiani MF, Pries AR, Hsu LL, Sarelius IH, and Cokelet GR (1994). Fluctuations in microvascular blood flow parameters caused by hemodynamic mechanisms. *Am J Physiol* **266**, H1822–H1828.

[150] Adair TH, Gay WJ, and Montani JP (1990). Growth regulation of the vascular system: evidence for a metabolic hypothesis. *Am J Physiol* **259**, R393–R404.

[151] Rubin P, and Casarett G (1966). Microcirculation of Tumors Part 1: anatomy, function and Necrosis. *Clin Radiol* **17**, 220–229.

[152] Hori K, Suzuki M, Tanda S, and Saito S (1999). *In vivo* analysis of tumor vascularization in the rat. *Jpn J Cancer Res* **81**, 279–288.

[153] Herbst RS, Takeuchi H, and Teicher BA (1998). Paclitaxel/carboplatin administration along with antiangiogenic therapy in non-small-cell lung and breast carcinoma models. *Cancer Chemother Pharmacol* **41**, 497–504.

[154] Teicher BA, Ara G, Buxton D, Leonard J, and Schaub RG (1998). Optimal scheduling of interleukin-12 and fractionated radiation therapy in the murine Lewis lung carcinoma. *Radiat Oncol Invest* **6**, 71–80.

[155] Kakeji Y, and Teicher BA (1997). Preclinical studies of the combination of angiogenic inhibitors with cytotoxic agents. *Invest New Drugs* **15**, 39–48.

[156] Teicher BA, Dupuis NP, Robinson MF, Emi Y, and Goff DA (1995). Antiangiogenic treatment (TNP-470/minocycline) increases tissue levels of anticancer drugs in mice bearing Lewis lung carcinoma. *Oncol Res* **7**, 237–243.

[157] Mauceri HJ, Hanna NN, Beckett MA, Gorski DH, Staba MJ, Stellato KA, Bigelow K, Heimann R, Gately S, Dhanabal M, Soff GA, Sukhatme VP, Kufe, DW, and Weichselbaum RR (1998). Combined effects of angiostatin and ionizing radiation in antitumour therapy. *Nature* **394**, 287–291.

[158] Hawighorst H, Knapstein PG, Knopp MV, Weikel W, Brix G, Zuna I,Schonberg SO, Essig M, Vaupel P, and van Kaick G (1998). Uterine cervical carcinoma: comparison of standard and pharmacokinetic analysis of time-intensity curves for assessment of tumor angiogenesis and patient survival. *Cancer Res* **58**, 3598–3602.

[159] Abramovitch R, Frenkiel D, and Neeman M (1998). Analysis of subcutaneous angiogenesis by gradient echo magnetic resonance imaging. *Magn Reson Med* **39**, 813–824.

[160] Griffiths JR, Taylor NJ, Howe FA, Saunders MI, Robinson SP, Hoskin PJ, Powell ME, Thoumine M, Caine LA, and Baddeley H (1997). The response of human tumors to carbogen breathing, monitored by Gradient-Recalled Echo Magnetic Resonance Imaging. *Int J Radiat Oncol Biol Phys* **39**, 697–701.

[161] Vaupel P (1992). Physiological properties of malignant tumours. *NMR Biomed* **5**, 220–225.